Oxidative dehydrogenation of propane over V/MCM-41 catalysts: comparison of O_2 and N_2O as oxidants

Evgueni V. Kondratenko [a,*], Maymol Cherian [a], Manfred Baerns [a], Dangsheng Su [b], Robert Schlögl [b], Xiang Wang [c], Israel E. Wachs [c]

[a] *Institute for Applied Chemistry Berlin-Adlershof, Richard-Willstätter-Str. 12, D-12489 Berlin, Germany*
[b] *Department of Inorganic Chemistry, Fritz-Haber-Institut der Max-Planck-Gesellschaft, Faradayweg 4-6, 14195 Berlin, Germany*
[c] *Operando Spectroscopy & Catalysis Laboratory, Department of Chemical Engineering, Lehigh University, Bethlehem, PA 18015, USA*

Abstract

A series of V/MCM-41 catalytic materials was synthesized by impregnation of MCM-41 and the addition of vanadium during the preparation of MCM-41. The nature and distribution of the VO_x species were studied by different spectroscopic techniques (TEM, TPR, in situ UV–vis, and in situ Raman). Highly dispersed VO_x species, which can be classified as monomeric and small two-dimensional VO_x aggregates, are present in materials with a vanadium loading of up to 5.3 wt% under conditions of the oxidative dehydrogenation of propane (ODP) and are independent of the preparation method. These VO_x species exhibit similar specific catalytic performance in the ODP reaction as a function of vanadium loading or apparent vanadium surface density. Crystalline V_2O_5 nanoparticles, however, are formed for 11.2 wt% V when the MCM-41 porous structure collapses. For all V/MCM-41 catalysts used in this study, higher propene selectivity is achieved with N_2O as compared with O_2 at similar degrees of C_3H_8 conversion. The catalytic activity is lower, however, in the presence of N_2O as compared with O_2 because of the weaker oxidizing potential of N_2O relative to O_2 for the re-oxidation of the reduced surface VO_x sites during the ODP reaction. There is no significant difference in propene selectivity between highly dispersed surface VO_x species and crystalline V_2O_5 nanoparticles when N_2O is used as an oxidant. In contrast to highly dispersed VO_x on the surface of MCM-41, the crystalline V_2O_5 nanoparticles are not selective for the ODP reaction in the presence of O_2. The positive effect of N_2O is related to the inhibition of direct C_3H_8 oxidation and the consecutive oxidation of C_3H_6 to CO_x. The inhibition is ascribed to reducing surface density (spatial separation) of active surface lattice oxygen in VO_x species, since N_2O is a weaker oxidant for re-oxidation of reduced VO_x species as compared with O_2. From a stoichiometric point of view of the ODP reaction, selective propene formation is favored over combustion reactions at lower surface densities.

© 2005 Elsevier Inc. All rights reserved.

Keywords: Oxidation; Dehydrogenation; O_2; N_2O; Propane; Propene; Vanadia; V_2O_5; Silica; MCM-41 support

1. Introduction

Conversion of low alkanes to value-added olefins, the building blocks of the petrochemical industry, by selective oxidative dehydrogenation reactions may become a potential economical route for their production in the coming years if selectivities and yields of olefins are significantly improved. The oxidative dehydrogenation of propane (ODP) to propene has been intensively investigated because of increasing world demand for propene. However, this reaction is kinetically limited for attaining high propene yields, since the selective reaction product, propene, is more reactive than propane and is easily combusted in the oxidizing environment [1]. Therefore, designing suitable catalysts and/or a suitable process environment is an important challenge for the coming years. Numerous catalytic systems have been evaluated for the ODP reaction, and the relevant results have

recently been reviewed [2,3]. Vanadium- and molybdenum-based catalytic materials are claimed to be most active and selective for the ODP reaction with O_2 [4–6]. Supported vanadium oxide catalysts have typically been found to be more selective than the unsupported bulk V_2O_5 material because of the interactions of VO_x species with the oxide support substrates (e.g., Al_2O_3, Nb_2O_5, TiO_2, ZrO_2, SiO_2, etc.) [7–9]. It has been reported that the interaction between the oxide support and the deposited vanadium oxide determines the structure of the resulting surface VO_x species [10]. Dehydrated surface VO_x species have been found to possess VO_4 coordination with one terminal V=O bond, with varying degrees of polymerization on the different supports. At high surface vanadium oxide coverage, crystalline V_2O_5 nanoparticles also exist. The catalytic activity in ODP and the propene selectivity are considered to be a function of these different vanadium oxide species and the specific support used. The factors that govern the catalytic performance of the surface VO_x species, however, are still being debated.

Recent studies of supported vanadium oxide on different mesoporous silicas have revealed that such materials are active and selective for the oxidative dehydrogenation of propane and ethane [11–15]. Mesoporous materials provide high surface areas and, hence, the potential for high dispersion of the catalytic active surface VO_x species. The rate of propene formation appears to vary with the dispersion of these species. Therefore the challenge is to achieve maximum dispersion of surface VO_x species. The overall performance of mesoporous supported vanadia catalysts for the ODP reaction is also a function of the chosen reaction conditions. The addition of small amounts of H_2O, CO_2, and N_2O to the ODP reaction feed [16–18] has been found to increase the propene selectivity at the expense of catalytic activity. When CO_2 was used as the oxidant, the propene selectivity over a gallium oxide catalyst was enhanced [19]. The use of CO_2 as an alternative oxidant, however, is limited by catalyst coking and by-product CO formation. Nitrous oxide was also applied as an oxidant for the ODP reaction over supported VO_x/γ-Al_2O_3 [20], resulting in an improved propene selectivity as compared with molecular oxygen. This finding suggests that N_2O may be promising as an oxidant for the ODP reaction.

Based on the above background, the present investigation is focused on understanding the influence of N_2O and O_2 as oxidants on the catalytic performance (activity and selectivity–conversion relationship) of supported V/MCM-41 catalytic materials for the ODP reaction. The effect of preparation methods and vanadium loadings on the distribution of VO_x species on the MCM-41 support among isolated surface VO_4 species, polymeric surface VO_4 species, and crystalline V_2O_5 nanoparticles will be elucidated with the application of different in situ spectroscopic methods. This molecular-level information will be used in deriving structure–reactivity–selectivity relationships of V/MCM-41 catalytic materials for the ODP reaction.

2. Experimental

2.1. Catalyst preparation

Two different preparation methods were chosen for deposition of vanadia on the mesoporous MCM-41 support prepared according to methods described in the literature [21]. One type of catalyst was prepared by impregnation of MCM-41 with a predetermined amount of vanadium acetyl acetate ($[CH_3COCH=C(O-)CH_3]_2VO$) in toluene. The final mixture was stirred at 300 K for 24 h, followed by filtering and washing of the impregnated catalyst with toluene to remove weakly bonded VO_x species. The resulting catalyst precursor was subsequently subjected to drying at 400 K for 12 h and calcination at 823 K for 12 h. The second type of catalyst was prepared with vanadyl sulfate ($VO(SO)_4$) dissolved in water that was mixed with tetraethylorthosilicate (TEOS) and cetyltrimethyl ammonium bromide (CTAB); the latter were templates used for the preparation of MCM-41 support. The resulting mixture was stirred for 24 h at 300 K and subjected to filtration, drying, and calcination as described above. Samples with different amounts of vanadium loadings varying from 0.2 to 11.2 wt% were synthesized. The catalysts are denoted here by their amount of vanadium loading [e.g., V(2.7)/MCM-41 contains 2.7 wt% V in the sample].

2.2. Catalyst characterization

The surface areas and the final vanadium contents were determined by BET and ICP analysis, respectively, after catalyst calcinations. The physical distribution of vanadium over the MCM-41 support was examined with TEM. The molecular distribution among the dehydrated isolated and polymeric surface VO_4 species and crystalline V_2O_5 was studied by in situ Raman and in situ UV–vis DRS. Crystalline V_2O_5 nanoparticles greater than 4 nm were subjected to XRD. The reducibility of VO_x species in the supported V/MCM-41 catalysts was investigated by in situ UV–vis DRS and H_2-TPR. A short description of each of the characterization methods and experimental procedures is given below.

Nitrogen physisorption was used to obtain specific surface areas in a single-point BET analyzer (Gemini III 2375, Micromeritics), with the use of N_2 physisorption at 77 K. The BET values are listed in Table 1. The method of Barret, Joyner, and Halenda (BJH) was used to determine the pore size distribution.

Inductively coupled plasma (ICP) measurements were used to determine the vanadium concentrations of each catalyst after calcination at 823 K. The final vanadium contents of the different catalysts are listed in Table 1.

Transmission electron microscopy (TEM) investigations of V/MCM-41 catalytic materials were performed for morphology determinations on a Philips CM 200 FEG field emission transmission electron microscope operated at 200 kV in vacuum.

Table 1
Vanadium content, BET surface area and average pore diameter of the synthesized catalysts

Method of catalyst preparation	Vanadium content (wt%)	S_{BET} (m^2/g)	Average pore diameter (Å)
Addition of vanadium during MCM-41 synthesis	0	1011	25.8
	0.2	1059	25.8
	0.6	892	26.2
	1.2	807	28.1
	2.7	871	27.8
	5.3	790	23.9
Impregnation of MCM-41 with vanadium	3.1	875	28
	4.1	836	27
	11.2	52	380

UV Raman spectra were collected with a Jobin Yvon Labram HR (high-resolution) spectrometer system with excitation at 325 nm (0.2 mW) and spectral resolution better than 2 cm^{-1}. The Raman system was equipped with a notch filter to reject the Rayleigh scattering down to ∼300 cm^{-1}. The scattered photons were directed and focused onto a single-stage monochromator, with 1800 grooves/mm, and a UV-sensitive CCD detector maintained at liquid-nitrogen temperature. The in situ Raman spectra were taken of the loose samples (10–20 mg) at room temperature after dehydration at 723 K in flowing oxygen (O$_2$/He = 20:80) in an environmental cell (Linkam, model T1600). Visible Raman spectra were collected with a Kaiser Optical Systems RXN spectrometer with excitation at 785 nm.

UV–vis DRS measurements were performed on a Cary 400 Varian spectrometer equipped with an in situ environmental cell (praying mantis, Harrick). The samples were diluted with Al$_2$O$_3$ in a 1:10 ratio. The samples for in situ measurements were pretreated in an O$_2$/N$_2$ (20% O$_2$) mixture at 773 K for 1 h. After this pretreatment, the in situ UV–vis DRS spectra of the catalytic materials were recorded at 773 K in an atmosphere of either hydrogen (H$_2$/N$_2$ = 10:90) or propane (C$_3$H$_8$/N$_2$0 = 10:90). The spectra were converted into the Kubelka–Munk function F(R).

X-ray diffraction (XRD) analyses were carried out with a STADIP transmission powder diffractometer (Stoe) with Cu-K$_{\alpha 1}$ radiation.

We made *H$_2$-TPR* measurements by heating 100 mg of sample at 20 K/min to 1073 K in a gas mixture of hydrogen (10 vol% in argon) with a total flow rate of 50 cm$^3_{STP}$/min. Hydrogen consumption was monitored by a thermal conductivity detector (TCD). Water formed or desorbed during TPR measurements was removed by a 4-Å molecular sieve before the flow entered the TCD. The hydrogen consumption was calibrated by argon pulses continuously introduced into the gas flow during sample heating.

2.3. Catalytic tests

A U-shaped fixed-bed quartz reactor (i.d. 5 mm) was used for the catalytic tests. The quartz reactor was immersed in a fluidized bed of sand serving as a source of heat. The temperature within the fixed bed of catalyst particles was measured with an axially movable thermocouple located inside a quartz capillary. Typically, 0.01–0.1 g of catalyst was diluted with similarly sized quartz particles and charged in the reactor for further temperature control. The oxidative conversion of propane was investigated with a feed of 40 vol% C$_3$H$_8$ and 40 vol% N$_2$O in Ne (C$_3$H$_8$/N$_2$O/Ne = 40:40:20) or 40 vol% C$_3$H$_8$ and 20 vol% O$_2$ in N$_2$ (C$_3$H$_8$/O$_2$/N$_2$ = 40:20:40) at 1 bar. Neon was used to control the formation of N$_2$ and O$_2$ in the case of N$_2$O decomposition. The total flow rate and the reaction temperature were varied between 30 and 240 cm$^3_{STP}$/min and 673 and 793 K, respectively. All V/MCM-41 catalysts were slightly deactivating during the first hour of time on stream with N$_2$O as oxidant. Characteristic reaction rates and product selectivities were only determined after pseudo-steady state was reached. The feed and products were analyzed with an online GC (HP 5800) equipped with Porapak Q and molecular sieve-5 columns. The contact times for kinetic measurements were adjusted to achieve propane conversions of less than 4%, which allowed for the determination of the initial propene selectivity and the initial rates of product formation. The rate of propene formation and turnover frequencie (TOFs) were calculated according to Eqs. (1) and (2), respectively. The rate unit is $n_{C_3H_6} \cdot \text{min}^{-1} \text{g}^{-1}$, where $n_{C_3H_6}$ is the number of propene moles, g refers to the catalyst, and TOF is the number of propene molecules formed per V atom and second.

$$r_{C_3H_6} = \frac{F_t}{22400 m_{cat}} C(C_3H_6), \tag{1}$$

$$TOF = \frac{r_{C_3H_6}}{60 n_V}, \tag{2}$$

where F_t is the total volumetric flow (cm$^3_{STP}$/min), m_{cat} is the catalyst mass (g), $C(C_3H_6)$ is the propene concentration at the reactor outlet (vol%), and n_V is the moles of vanadium per gram of catalyst (mol/g).

3. Results

The following three sections describe the results of physical and chemical characterization of the supported V/MCM-41 catalytic materials. The catalytic performance of these materials in the oxidative dehydrogenation of propane in the presence of O$_2$ and N$_2$O is subsequently presented.

3.1. Morphology of V/MCM-41 materials as a function of V content and preparation method

The specific surface areas (S_{BET}) of the catalytic materials and the pure MCM-41 support are listed in Table 1. There is only a slight decrease in S_{BET} of the supported V/MCM-41 catalysts for vanadium loadings up to 5.3 wt%. This is valid for both supported V/MCM-41 and materials prepared by vanadium addition during synthesis of MCM-41.

S_{BET} of V(11.2)/MCM-41 is significantly lower than that of the other catalytic materials, indicating that the microstructure of MCM-41 is influenced by the comparatively high vanadium loading. The average pore size was calculated to be ∼2.7 nm for all of the catalytic materials, with the exception of V(11.2)/MCM-41. Thus, the mesoporous structure of the support was preserved in most of the synthesized materials. This conclusion is further supported by the results of the morphology as obtained by TEM measurements (Fig. 1); the TEM image of the supported V(0.2)/MCM-41 catalyst is shown in Fig. 1a, where the micrograph was taken with an electron beam parallel to the pores. The TEM image reveals that the highly ordered nanoporous structure of MCM-41 is preserved after it is loaded with vanadium oxide. Although X-ray energy-dispersive spectroscopy with the TEM reveals the presence of vanadium, the absence of any vanadium oxide contrast in Fig. 1a indicates that vanadium oxide must be present in a dimension of less than 1 nm that is not detectable in the TEM image. With increased vanadium loading, no significant changes in the structure of MCM-41 or in the vanadium distribution are observed (Fig. 1b). Higher load-

ings of vanadium cause a dramatic change in the MCM-41 structure, as shown for V(11.2)/MCM-41 in Fig. 1c: (i) all of the nanoporous channels disappear; (ii) the MCM-41 structure undergoes a morphological change by agglomeration to large debris, giving the *polymer*-like contrast in Fig. 1c; and (iii) V_2O_5 crystals as large as several tens of nanometers are found in this sample. These morphological changes result in a dramatic drop of S_{BET} from 800–900 m^2/g to 52 m^2/g (see Table 1).

The effect of vanadium loading on the crystallization of V/MCM-41 materials was also investigated by powder XRD. For samples with vanadium loading up to 5.3 wt%, no spectral features indicating the presence of crystalline V_2O_5 are present. This may be understood either as the presence of small crystalline nanoparticles (<4 nm) or as surface VO_x species that cannot be detected by XRD because of the absence of long-range order. Intense reflexes corresponding to crystalline V_2O_5 are visible, however, in the XRD patterns of V(11.2)/MCM-41 (Fig. 2), which is in agreement with the TEM observation shown in Fig. 1c. Raman and UV–vis spectroscopic characterization studies were
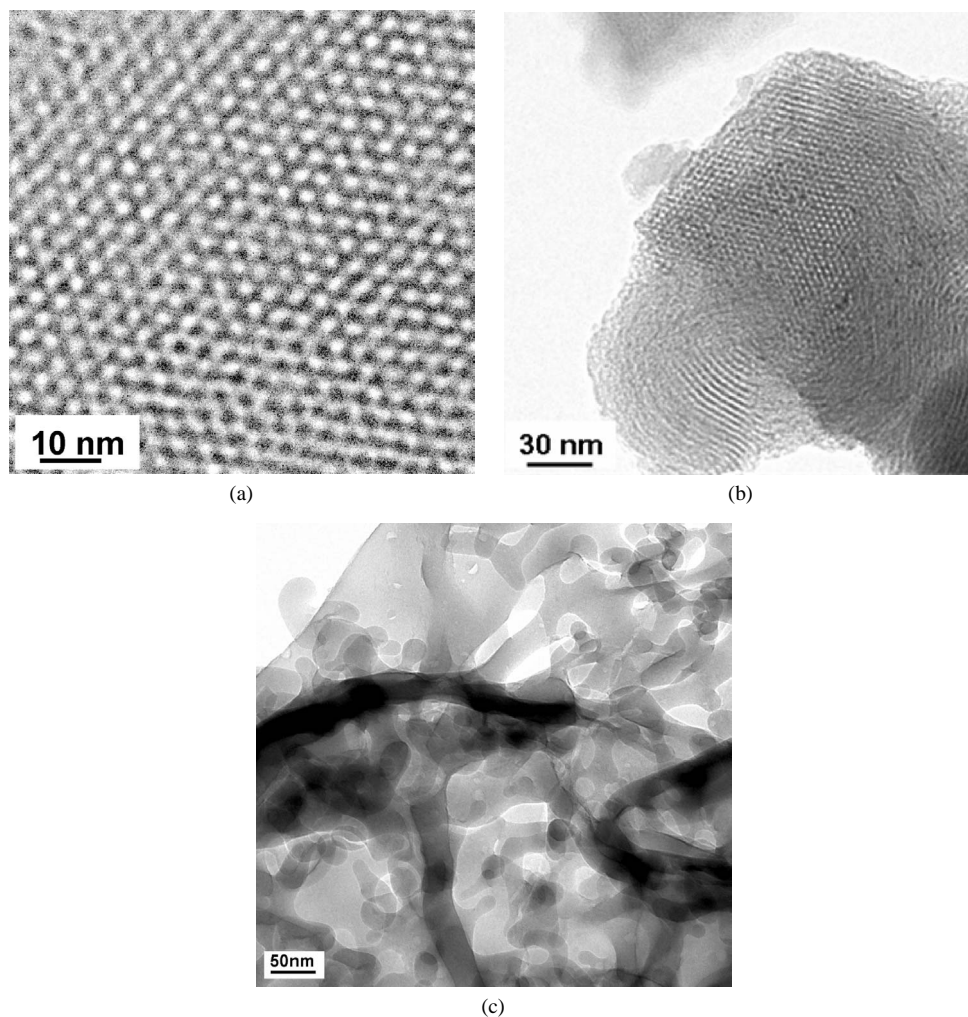

(a)

(b)

(c)

Fig. 1. TEM micrographs of the V/MCM-41 samples taken with the electron beam parallel to the pores: V(0.2)/MCM-41 (a), V(2.5)/MCM41 (b) and V(11.2)/MCM-41 (c).
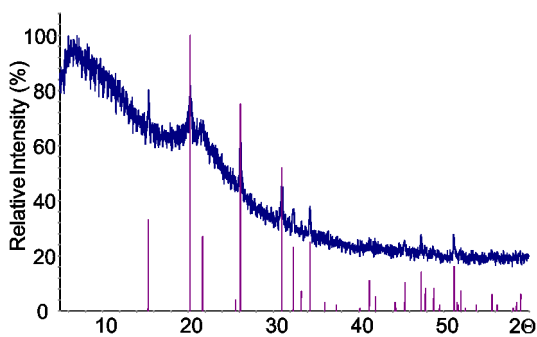
Fig. 2. Powdered X-ray diffraction patterns of V(11.2)/MCM-41.

also undertaken to obtain more definitive information about the possible presence of XRD-amorphous crystalline V_2O_5 nanoparticles and surface VO_x species for samples possessing up to 5.3 wt% V.

3.2. Determination of different VO_x molecular structures and their partitioning in V/MCM-41

A comparison of the in situ UV–vis spectra of the V/MCM-41 samples investigated is shown in Fig. 3. The spectra were taken at 773 K in a flow of O_2 (O_2/N_2 = 20:80). Under such conditions water is released from the coordination sphere of V^{5+}, leaving behind tetrahedrally coordinated V^{5+}. The spectra are essentially the same for all dehydrated V/MCM-41 catalysts, with the exception of the highly loaded V(11.2)/MCM-41 sample, which also contains XRD-detectable crystalline V_2O_5 (Section 3.1, Fig. 2). The absorption at 295 nm and its correspondingly high band-gap energy value ($E_g \sim 3.4$ eV) are characteristic of isolated dehydrated surface VO_4 species [22]. In order to derive more precise insights into the structure of VO_x species in low loaded ($\leqslant 5$ wt%) V/MCM-41 samples, their UV/vis spectra were compared with those of magnesium vanadates with structures of $Mg_3V_2O_8$ and $Mg_2V_2O_7$, where isolated VO_4 units and VO_x species with V–O–V bonds, respectively,
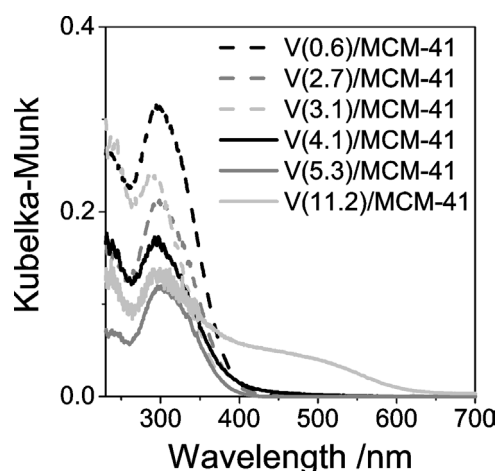
are present. Fig. 4 compares these spectra. It is clear that spectra of low loaded ($\leqslant 5$ wt%) V/MCM-41 samples differ from that of pure $Mg_3V_2O_8$, but they are similar to that of a mixture of $Mg_3V_2O_8$ and $Mg_2V_2O_7$. Taking into account these experimental observations, it is concluded that both isolated VO_4 units and small VO_x aggregates that have V–O–V bonds are present on the surface of the low loaded ($\leqslant 5$ wt%) V/MCM-41 samples. Here the above VO_x species are referred to as highly dispersed. Increasing the vanadium content to 11.2 wt% gives rise to a new broad UV–vis band between 400 and 600 nm, with a corresponding low band-gap energy value ($E_g \sim 2.9$ eV) characteristic of crystalline V_2O_5 [23].

The in situ Raman spectra of the V/MCM-41 catalysts, after dehydration at 723 K, are compared in Fig. 5. The spectra in Figs. 5a and 5b were taken under 325 and 785-nm excitation. The band at ~ 477 cm^{-1} originated from vibrations of Si–O–Si rings of the MCM-41 support, and the band at ~ 1031 cm^{-1} is associated with dehydrated, highly dispersed surface $O=V(–O–Si)_3$ species [24–26]. However, recent theoretical and experimental studies on Raman spectra of V/SiO2 provide an indication that the band at ~ 1031 cm^{-1} cannot be assigned to vanadyl species exclusively [27]. Since no Raman band at ~ 966 cm^{-1} was identified, according to [28] the highly dispersed surface VO_x species are concluded to be in non-framework sites. The absence of a sharp Raman band at ~ 994 cm^{-1}, with its multiple associated sharp bands at lower wave numbers, demonstrates that crystalline V_2O_5 nanoparticles are not present in any of the V/MCM-41 samples with vanadium loadings up to 5 wt%. This band was identified in V(11.2)/MCM-41 only (Fig. 5). Since polymeric VO_x species can easily be detected under visible excitation [28], in contrast to isolated vanadyl species, Raman spectra of V(5.3)/MCM-41 and V(11.2)/MCM-41 samples were collected at 785-nm excitation. The respective spectra are given in Fig. 5b. This figure shows nicely that crystalline V_2O_5 nanoparti-

Fig. 3. UV/vis-DRS spectra of different V/MCM-41 materials during pre-treatment in an O_2/N_2 = 20:80 mixture at 773 K.
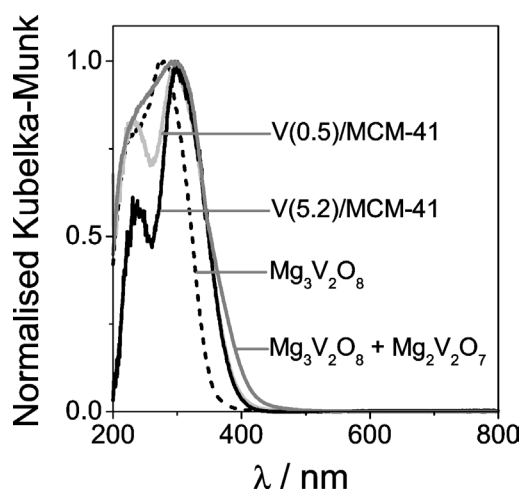

Fig. 4. UV/vis-DRS spectra of V(0.5)/MCM-41 and V(5.3)/MCM-41 materials as well as $Mg_3V_2O_8$ and $Mg_2V_2O_7$.
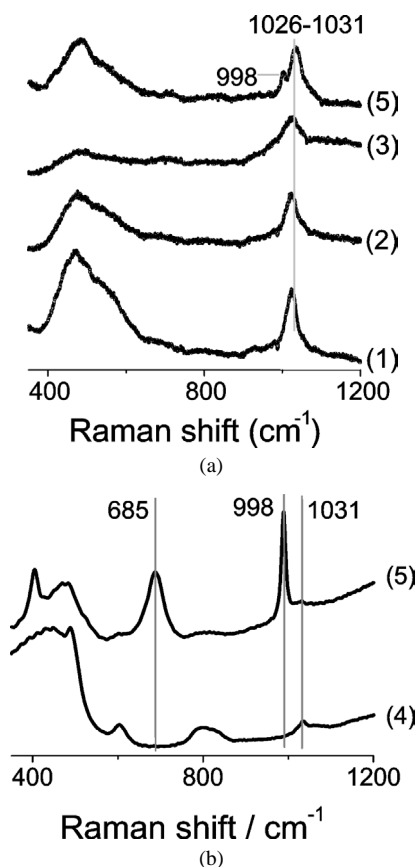
Fig. 5. Raman spectra of different V/MCM-41 materials under dehydrated conditions with 325 (a) and 785 (b) nm excitation wavelengths: (1) V(0.2)/MCM-41, (2) V(2.1)/MCM-41, (3) V(4.1)/MCM-41, (4) V(5.3)/MCM-41, (5) V(11.2)/MCM-41.

cles in the V(11.2)/MCM-41 sample are strongly resonance-enhanced under visible laser excitation. Since no signs of the presence of crystalline V_2O_5 nanoparticles was found in V(5.3)/MCM-41 even under visible laser excitation, it is concluded that V/MCM-41 samples with vanadium loading lower than 5.3 wt% are free of crystalline V_2O_5 nanoparticles.

3.3. Redox properties

The in situ UV–vis spectra obtained after reduction of fully oxidized V(2.7)/MCM-41 by C_3H_8 or H_2 at 773 K are presented in Fig. 6. The intensity of the ligand-to-metal charge transfer (LMCT) bands in the 200–400-nm region decreases upon exposure to the reducing C_3H_8 and H_2 because of reduction of the V^{5+} to V^{4+} or V^{3+}. The UV–vis bands for surface V^{4+} and/or V^{3+} species arise from d–d transitions and appear as broad and weak features in the 400–700-nm region (note the nonzero value of the absorption for the reduced samples in this region) [22,29]. The reduced samples were subjected to re-oxidation by oxygen. The reduced surface VO_x species are easily re-oxidized to the surface V^{5+} species, but the re-oxidation is incomplete for the chosen experimental conditions (see Fig. 6). Similar
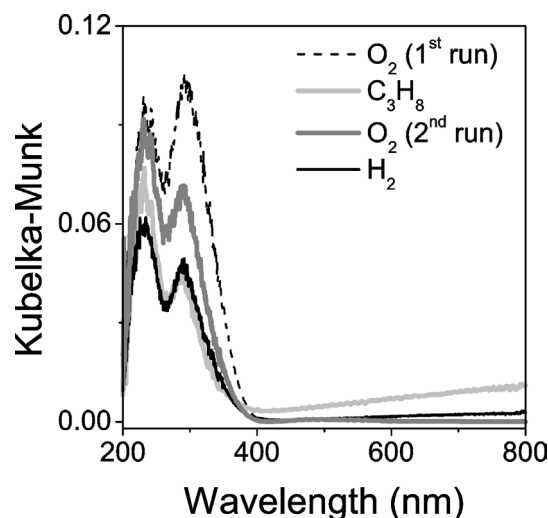

Fig. 6. UV/vis spectra under oxidation and reduction environment at 773 K ($O_2/N_2 = 20{:}80$, $C_3H_8/N_2 = 10{:}90$ and $H_2/N_2 = 10{:}90$).
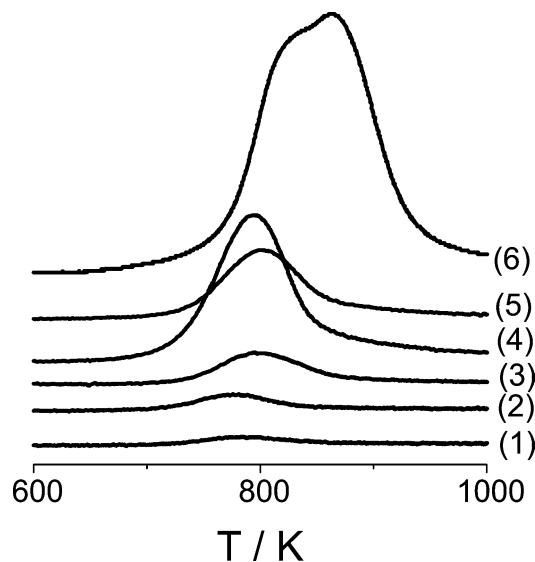

Fig. 7. H_2-TPR spectra for differently prepared V/MCM-41 catalytic materials as a function of V loading: (1) V(0.2)/MCM-41, (2) V(0.6)/MCM-41, (3) V(1.2)/MCM-41, (4) V(3.1)/MCM-41, (5) V(2.7)/MCM-41, (6) V(11.2)/MCM-41.

results are also characteristic for all of the V/MCM-41 catalysts.

The H_2-TPR spectra of the V/MCM-41 materials are shown in Fig. 7. T_{max}, which qualitatively reflects the reducibility of the supported vanadia, increases slightly from 778 to 793 K as the vanadium loading increases from 0.2 to 5.3 wt% for the samples prepared by the addition of vanadium during synthesis of MCM-41. For the impregnated samples, T_{max} is slightly higher and around 808 K. These slight shifts to higher T_{max} are a consequence of the higher H_2O partial pressures formed with higher V-loaded samples that retard the reduction process. The single T_{max} obtained for all samples represents a single stage reduction of the surface V^{5+} to surface V^{3+} [29–31]. The H_2-TPR profile for
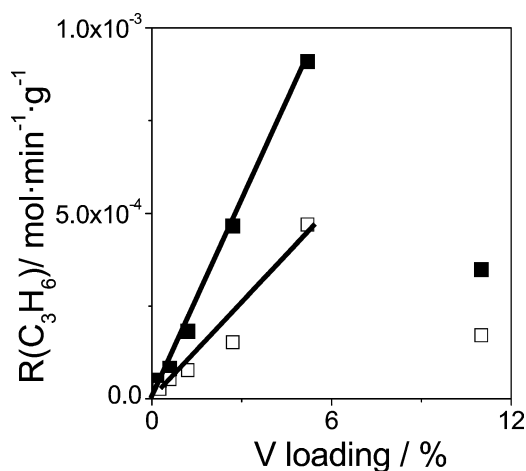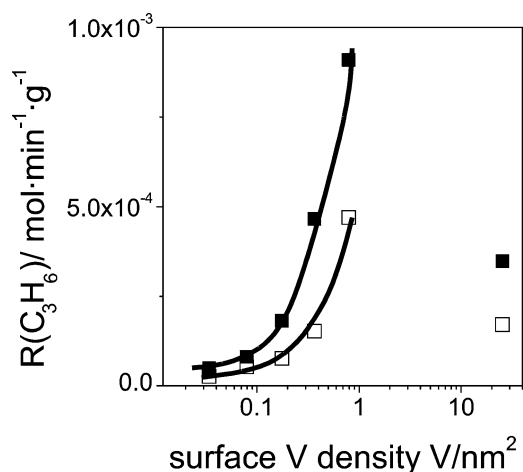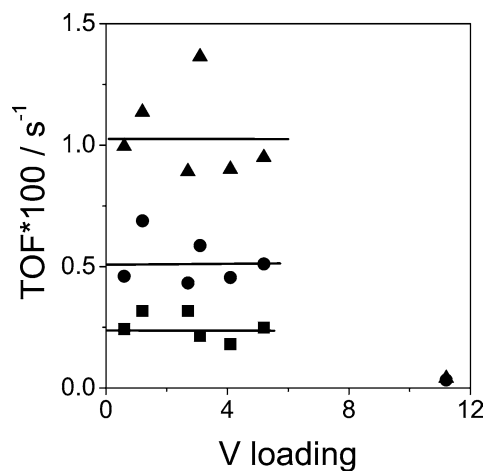
Fig. 8. Rates of propene formation versus vanadium loading (a) and apparent vanadium surface density (b) at 748 K using $C_3H_8/O_2/N_2 = 40:20:40$ (closed symbols) and $C_3H_8/N_2O/N_2 = 40:40:20$ (open symbols) mixtures.
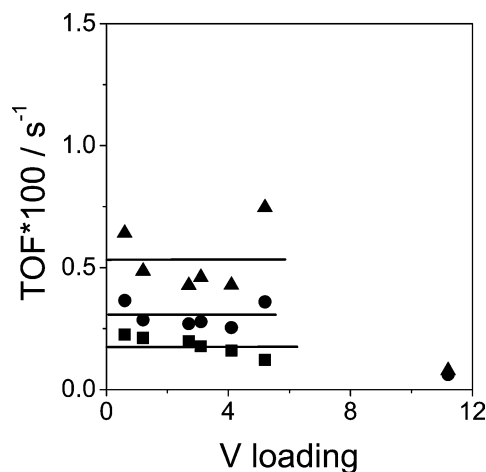

Fig. 9. TOF of propene formation at 698 (●), 723 (■) and 748 (▲) K versus vanadium loading using $C_3H_8/O_2/N_2 = 40:20:40$ (a) and $C_3H_8/N_2O/N_2 = 40:40:20$ (b) mixtures.

V(11.2)/MCM-41 has an additional shoulder with a maximum shifted to higher temperatures due to the presence of crystalline V_2O_5 nanoparticles in this sample. Higher T_{max} for crystalline V_2O_5 than for the surface VO_x species arises from the more difficult reduction of the internal V^{5+} sites in the V_2O_5 crystalline lattice during H_2-TPR.

3.4. Catalytic performance of V/MCM-41 materials with O_2 and N_2O

C_3H_6, CO, and CO_2 were the main reaction products, with oxygen and nitrous oxide as oxidants in the ODP reaction over the differently loaded and prepared V/MCM-41 catalytic materials. Very small amounts (<0.01 vol%) of acetaldehyde and acrolein were also produced as reaction by-products. V loading, method of catalyst preparation, and the oxidant were examined for their influence on the rate of propene formation (C_3H_6 mol/(min g)), with oxygen and nitrous oxide as oxidants. The corresponding activity results are plotted in Figs. 8a and 8b as a function of the V con-

tent and apparent V surface density, respectively. These results reveal that the activity for propene formation is higher with O_2 than with N_2O for all vanadium loadings or surface densities. Regardless of the oxidizing agent, the activity increases with increasing vanadium loading up to 5.3 wt% (ca. 1 V/nm^2). There is no significant difference in the rates of propene formation for samples prepared by different methods. This indicates a similarity of VO_x species in differently prepared V/MCM-41 materials. To understand the intrinsic activity of surface VO_x species, we calculated the turnover frequency (TOF) (presented in Fig. 9) according to Eq. (2). The nearly constant TOF values for the catalysts with vanadium loadings of up to 5.3 wt% (V surface density is below ca. 1 V/nm^2) suggest that all of the surface VO_x sites are essentially identical. V(11.2)/MCM-41 has the lowest TOF value because of formation of sintered V_2O_5 nanoparticles (dispersion <100%). The catalytic ODP reaction is sensitive to the specific oxidant, and lower TOF values were obtained with N_2O than with O_2. This observation is discussed in detail in Section 4.1.
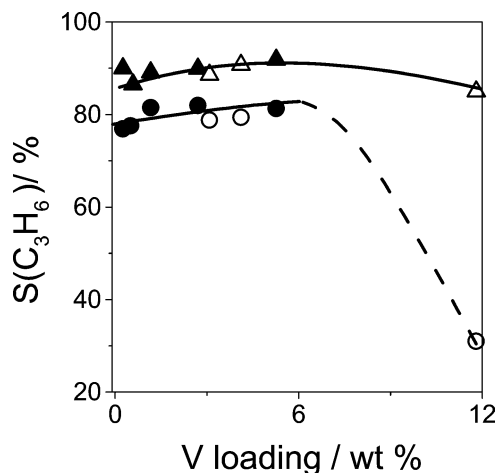
Fig. 10. C_3H_6 selectivity at low degrees of propane conversion (∼2%) at 748 K versus vanadium loading using $C_3H_8/O_2/N_2 = 40{:}20{:}40$ (circles) and $C_3H_8/N_2O/N_2 = 40{:}40{:}20$ (triangles) mixtures. Open symbols are for materials prepared by impregnation, solid symbols are for materials prepared with vanadium addition during MCM-41 synthesis.

The effect of vanadium loading and type of oxidant on propene selectivity at a degree of propane conversion of ca. 2% is shown in Fig. 10. The selectivity increases slightly with an increase in vanadium loading of up to 5.3 wt% and decreases with a further increase in vanadium loading; the selectivity maximum is difficult to define because of the lack of experimental data. This is valid for catalytic tests with

both N_2O and O_2. However, for an N_2O-containing mixture this decrease is not as clear as that for an O_2-containing reaction feed. It should also be emphasized that the propene selectivity with N_2O is slightly higher over all of the catalysts than that with O_2. Further studies were made to understand the reaction pathways for ODP; the ODP tests were conducted with N_2O and O_2 at different contact times (i.e., different degrees of propane conversion). The selectivity–conversion relationships for different catalysts in the presence of O_2 and N_2O are compared in Fig. 11. The propene selectivity decreases whereas CO and CO_2 selectivities increase with increasing propane conversion for both oxidants. The relationship obtained indicates the secondary nature for CO_x formation, that is, CO and CO_2 are formed via consecutive C_3H_6 oxidation. Taking into account this finding and the non-zero CO and CO_2 selectivities at near-zero C_3H_8 conversion, it is suggested that both CO_2 and CO can also be primary products of total propane oxidation. However, this reaction pathway plays a significant role at low degrees (<2%) of propane conversion only. The contribution of the consecutive C_3H_6 oxidation to total CO_x production increases strongly with a progressive increase in C_3H_8 conversion and prevails at high degrees. From a more detailed analysis of the results in Fig. 11 it is concluded that CO formation is more strongly influenced by the degree of C_3H_8 conversion as compared with CO_2 formation. For an O_2-containing feed, relative changes in CO selectivity over V(2.7)/MCM-
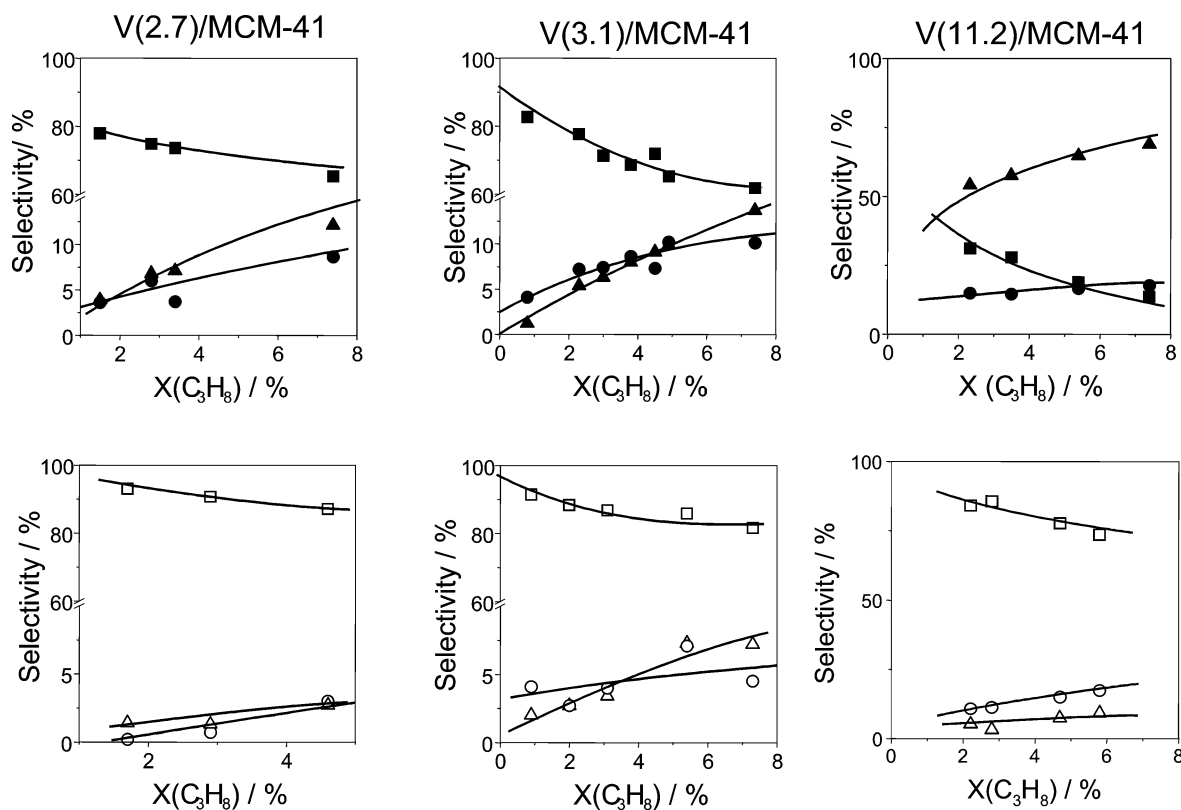

Fig. 11. C_3H_6 (■,□), CO (▲,△) and CO_2 (●,○) selectivities versus propane conversion at 773 using $C_3H_8/O_2/N_2 = 40{:}20{:}40$ (solid symbols) and $C_3H_8/N_2O/N_2 = 40{:}40{:}20$ (open symbols) mixtures.
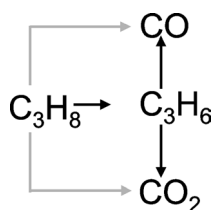
Fig. 12. Suggested reaction scheme of propane oxidation. Solid black arrows represent main reactions, while the grey arrows represent minor reaction pathway.

41, V(3.1)/MCM-41, and V(11.2)/MCM-41 are 13, 8, and 15% as C_3H_8 conversion is increased from 0.8 to 7.6, from 1.5 to 7.4, and from 2 to 7.5, respectively. The respective changes in CO_2 selectivity are 6, 5, and 2.7%. From a comparison of the relative changes in CO and CO_2 selectivities, it is obvious that CO selectivity as compared with that of CO_2 is a stronger function of the degree of C_3H_8 conversion. Thus it is concluded that propene is largely oxidized to CO as compared with CO_2. The extent of the decrease in propene selectivity, however, is smaller with N_2O than that with O_2. For similar propane conversions, the selectivity for carbon oxides is ca. 2–3 times higher with O_2 than with N_2O. The above observations suggest a complex reaction scheme of parallel and consecutive steps for the ODP reaction using either O_2 or N_2O; the scheme is presented in Fig. 12.
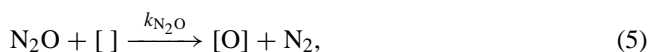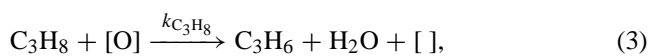
4. Discussion

4.1. Nature of surface VO_x species and their relationship to the activity and selectivity in the ODP reaction

The results for materials characterization revealed that highly dispersed surface VO_x species are present in the supported V/MCM-41 catalysts up to 5 wt% V. These species reside in extra-framework positions, since the characteristic 960 cm^{-1} band typical for framework cations in siliceous molecular sieves [28] is not observed for the supported V/MCM-41 catalysts. The molecular structure of the surface VO_x species on MCM-41 is independent of the synthesis method, since the same structure results from either incorporation of vanadium during the MCM-41 synthesis process or by post-impregnation of the formed MCM-41 support with vanadium (Section 3.2). This agrees well with previously reported results on the characterization of V/MCM-41 [13, 32], V/MCM-48 [22], and V/HSM silica [33]. The Raman spectra suggest that all of the vanadia species are located in accessible surface sites, since these dehydrated sites readily become hydrated upon exposure to ambient air [29]. The V(11.2)/MCM-41 sample, however, consists of a collapsed MCM-41 structure and crystalline V_2O_5 nanoparticles.

The experimental data showed that the catalytic performance (i.e., activity and the relationship between propene selectivity and propane conversion) of V/MCM-41 catalysts

in the oxidative dehydrogenation of propane depends on the distribution of VO_x species on the catalyst surface and the nature of the oxidant. From Fig. 10 it can be seen that the propene selectivity at a propane conversion of ca. 2% increases slightly with vanadium loadings up to 5.3 wt% for both oxidants. The weak differences in C_3H_6 selectivity of catalysts with low vanadium loadings (up to 5.3 wt%) is a strong indication of the participation of surface VO_x species of the same nature in C_3H_8 activation yielding C_3H_6. This is supported by the results from characterization techniques, such as UV–vis and Raman spectroscopy (Section 3.2), which demonstrate the presence of highly dispersed surface VO_x in these samples. For V(11.2)/MCM-41, which possesses crystalline V_2O_5 nanoparticles (Section 3.2), there is only a slight decrease in propene selectivity from ca. 90 to 85% when N_2O is used, whereas for O_2 there is a marked decrease from ca. 80 to 30% at comparable degrees of propane conversion. A possible reason for these phenomena is presented and discussed in Section 4.2.

As shown in Fig. 8, the rate of C_3H_6 formation and the TOF values are lower with N_2O than with O_2 as the oxidant. This can be explained in the following way. It is commonly accepted that the ODP reaction over vanadia-based catalysts proceeds via a Mars–van Krevelen mechanism. This mechanism suggests that C_3H_8 removes lattice oxygen from VO_x species, yielding C_3H_6, H_2O, and a reduced VO_x center (Eq. (3)). Subsequently, the lattice oxygen is replenished by gas-phase oxygen in a re-oxidation step (Eq. (4)). In the case of N_2O, the catalyst re-oxidation proceeds according to Eq. (5). The reaction steps involved are assumed to be irreversible. In our previous work on the ODP reaction over VO_x/γ-Al_2O_3, it was shown that the same oxygen species, lattice oxygen of vanadia, is formed from O_2 and N_2O [20].

$$C_3H_8 + [O] \xrightarrow{k_{C_3H_8}} C_3H_6 + H_2O + [\ ], \tag{3}$$

$$O_2 + 2[\ ] \xrightarrow{k_{O_2}} 2[O], \tag{4}$$

$$N_2O + [\ ] \xrightarrow{k_{N_2O}} [O] + N_2, \tag{5}$$

where [O] stands for the lattice oxygen of VO_x and [ ] corresponds to an anion vacancy after removal of lattice oxygen from VO_x species. Under steady-state conditions and in the presence of O_2 and N_2O, the rate of C_3H_6 formation can be described as follows:

$$r_{C_3H_6}^{O_2} = k_{C_3H_8} p(C_3H_8) \left[\frac{1}{1 + \frac{k_{C_3H_8} p(C_3H_8)}{k_{O_2} p(O_2)}} \right], \tag{6}$$

$$r_{C_3H_6}^{N_2O} = k_{C_3H_8} p(C_3H_8) \left[\frac{1}{1 + \frac{k_{C_3H_8} p(C_3H_8)}{k_{N_2O} p(N_2O)}} \right]. \tag{7}$$

In addition to the product of the C_3H_8 partial pressure and the reaction constant of propane activation, Eqs. (6) and (7) include a complex expression (squared brackets). Since the product of the C_3H_8 partial pressure and the reaction constant of propane activation is the same in Eqs. (6) and

(7), it cannot be responsible for differences in the rates of C_3H_6 formation with O_2 and N_2O (Fig. 8). Therefore, the expression in squared brackets contains information on factors influencing the catalytic activity with both O_2 and N_2O. The lower the denominator in this expression, the higher is the rate of propene formation. Two experimental facts should be taken into account: (i) $k_{C_3H_8}$ is the same for O_2- and N_2O-containing mixtures; and (ii) the ratios of $p(C_3H_8)/p(O_2)$ and $p(C_3H_8)/p(N_2O)$ are 2 and 1, respectively. From Eqs. (6) and (7) and the two above facts, a lower reaction rate with O_2 as compared with N_2O would be expected if k_{N_2O} and k_{O_2} were the same or k_{N_2O} were greater than k_{O_2}. However, it would contradict the experimental observations in Figs. 8 and 9. Therefore, the lower rate of C_3H_6 formation in the presence of N_2O as compared with that in the presence of O_2 is related to the lower ability of N_2O to re-oxidize the reduced surface VO_x sites. Previously, this low activity of N_2O was experimentally proved for differently loaded catalytic materials of the type VO_x/γ-Al_2O_3 [20]. Taking this into account, the lower intrinsic activity (TOF) of VO_x species for C_3H_8 activation with N_2O than with O_2 (see Fig. 9) can be explained as follows. For the calculation of TOF values, the total number of vanadium atoms (including those in the bulk) was used without consideration of the fact that not vanadium atoms, but the lattice oxygen of VO_x species, participates in C_3H_8 activation. According to Eqs. (3)–(7), the steady-state concentration of lattice oxygen is a function of the rates of catalyst reduction and re-oxidation. Since the rate of catalyst re-oxidation by N_2O is slower than that by O_2, a lower steady-state concentration of lattice oxygen is expected to be responsible for C_3H_8 activation in the presence of N_2O. Therefore, the TOF values presented in Fig. 9 do not reflect the discrepancy in the intrinsic activity of VO_x species for the ODP reaction with O_2 and N_2O, but the difference in the ability of the catalyst for its re-oxidation by different oxidants, that is, differences in steady-state concentrations of lattice oxygen in the presence of two different oxidants. Thus, it is concluded that the intrinsic activity of VO_x species does not depend on the oxidant used, and the rate of re-oxidation by the oxidants is responsible for the different ODP reactivities with O_2 and N_2O.

4.2. Role of oxidant in selective and non-selective routes of ODP

As shown in Section 3.4, the selectivity (distribution of products) of the ODP reaction strongly depends on the nature of the oxidant applied (Figs. 10 and 11). Although propene is the main olefin with both N_2O and O_2, the propene selectivity achieved is lower when O_2 is used as the oxidant as compared with N_2O. Similar results were previously reported in [20] for the oxidative dehydrogenation of propane over differently loaded VO_x/γ-Al_2O_3 catalytic materials. Two important improving effects of N_2O on the ODP reaction should be especially emphasized: (i) a higher pri-
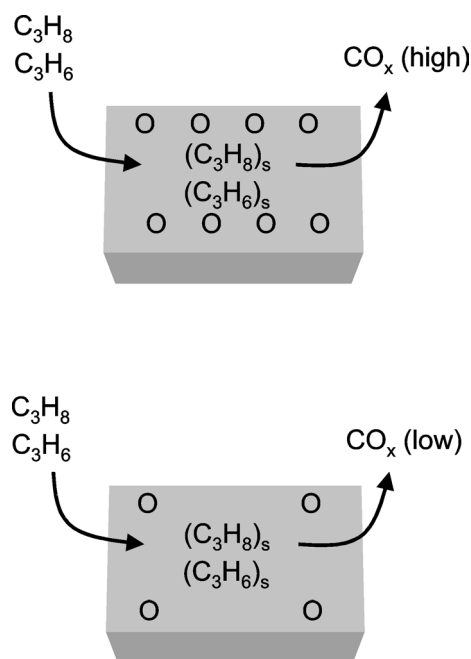

Fig. 13. Schematic presentation of the role of lattice oxygen isolation in CO_x formation.

mary C_3H_6 selectivity is achieved, and (ii) the decrease in C_3H_6 selectivity with increasing degree of propane conversion is less marked.

This effect of the oxidant on the catalytic performance can be associated with the activation of the oxidant. As discussed in Section 4.1, N_2O re-oxidizes reduced VO_x sites more slowly as compared with O_2, yielding a lower concentration of active lattice oxygen and, therefore, its lower density. From the stoichiometric requirements of the ODP reaction it is postulated that one selective catalyst site should contain one to two active lattice-oxygen anions to obtain the desired propene. Active sites with more than two active lattice oxygen anions would favor the formation of waste products (i.e., CO and CO_2) by consecutive total oxidation steps. Since several oxygen species are needed for CO_x formation in contrast to C_3H_6 formation, the latter reaction pathway prevails at low densities/concentrations of active oxygen species. This is schematically illustrated in Fig. 13. According to this figure, CO_x formation is favored at high densities of active lattice oxygen in VO_x surface species. Such a situation occurs when the rate of catalyst re-oxidation (Eqs. (4) and (5)) is faster than that of reduction (Eq. (3)). As discussed in Section 4.1, N_2O re-oxidizes reduced VO_x sites more slowly as compared with O_2, yielding a lower concentration of active lattice oxygen; that is, its surface density is lower. This is particularly valid for V(11.2)/MCM-41, since it has the highest surface density of lattice oxygen in the presence of O_2 and, respectively, the lowest propene selectivity. The influence of the surface density of active lattice oxygen in VO_x species on propene selectivity is clearly visible for this catalyst as compared with other materials (Figs. 10 and 11). Thus, spatial separation of active lattice

oxygen anions from each other on the catalyst surface favors propene formation and simultaneously minimizes its further oxidation to CO_x. Such a hypothesis of active site isolation in selective oxidation of hydrocarbons was first formulated and published by Callaham and Grasselli [34]. However, in the present discussion, it cannot be excluded that in addition to lattice oxygen, adsorbed oxygen species also participate in the oxidation of surface intermediates to CO_x, as recently shown for a complex mixed-oxide catalyst [35]. In this case, active sites containing one to two lattice oxygen anions may become active for CO_x formation, if additional adsorbed oxygen species are formed in the vicinity of these selective active sites. A detailed understanding of the role of adsorbed oxygen species is still needed and is currently being worked on.

5. Summary and conclusions

The findings from the present investigation can be summarized as follows:

1. Combination of the characterization results obtained by different techniques (TEM, TPR, in situ UV/vis DRS, and Raman spectroscopy) for vanadia supported on high-surface-area mesoporous MCM-41 reveals that the nature and distribution of VO_x species do not depend on vanadium loading up to at least 5.3 wt%. In these samples the VO_x surface species are highly dispersed as monomeric and small surface VO_x clusters under conditions of the oxidative dehydrogenation of propane (ODP). Crystalline V_2O_5 nanoparticles are formed on V/MCM-41 with 11.2 wt% vanadium when the mesoporous structure collapses.

2. Regardless of vanadium loading (up to 5.3 wt%), the highly dispersed surface VO_x species show similar intrinsic catalytic activity. However, the measured activity of these species is lower when N_2O is used as the oxidant, in comparison with O_2. The difference is due to the lower ability of N_2O to re-oxidize reduced VO_x species rather than re-oxidation by O_2.

3. In contrast to highly dispersed surface VO_x species, the crystalline V_2O_5 nanoparticles are not selective when O_2 is used as the oxidant. However, in the presence of N_2O, there is no strong difference in propene selectivity.

4. For all of the V/MCM-41 materials, the use of N_2O instead of O_2 favors selective propane oxidation to propene over the total combustion of propane or propene. The improving effect of N_2O is related to site isolation of the active surface lattice oxygen species; thereby the direct deep propane and consecutive propene oxidation to CO_x is inhibited.

5. For catalyst design it appears important to ascertain a high dispersion of the reducible metal oxides (MeO_x) on an inert support. These metal oxides should be easily reduced by hydrocarbon rather than re-oxidized by an oxidant. This will spatially isolate active lattice oxygen species in MeO_x aggregates favoring selective oxidation over a combustion reaction. With respect to process design, it is well known that N_2O is also a suitable oxidant for selective benzene oxidation to phenol. Whether such a process operation can be also applied to selective alkane oxidation remains to be seen. Moreover, activity and selectivity improvements need to be made, the availability of N_2O in sufficient quantities has to be ascertained, and, finally, process economics must be studied.

References

[1] H.H. Kung, Adv. Catal. 40 (1994) 1.
[2] O.V. Buyevskaya, M. Baerns, Catalysis 16 (2002) 155.
[3] M. Baerns, G. Grubert, E.V. Kondratenko, D. Linke, U. Rodemerk, Oil Gas-Eur. Mag. 1 (2003) 36.
[4] R.B. Watson, U.S. Ozkan, J. Catal. 191 (1999) 12.
[5] Y. Liu, G. Zhou, M. Xian, Y. Bi, K. Zhen, React. Kinet. Catal. Lett. 73 (2001) 199.
[6] C. Pak, A.T. Bell, T.D. Tilley, J. Catal. 206 (2002) 49.
[7] X. Gao, Q. Xin, X. Guo, Appl. Catal. A 114 (1994) 197.
[8] T.C. Watling, G. Deo, K. Seshan, I.E. Wachs, J.A. Lercher, Catal. Today 28 (1996) 139.
[9] T. Blasco, A. Galli, J.M. López-Nieto, F. Trifiro, J. Catal. 169 (1997) 203.
[10] A. Khodakov, B. Olthof, A.T. Bell, E. Iglesia, J. Catal. 181 (1999) 205.
[11] J.M. López-Nieto, Top. Catal. 15 (2001) 189.
[12] O.V. Buyevskaya, A. Brückner, E.V. Kondratenko, D. Wolf, M. Baerns, Catal. Today 67 (2001) 369.
[13] B. Solsona, T. Blasco, J.M. López-Nieto, M.L. Pena, F. Rey, A. Vidal-Moya, J. Catal. 203 (2001) 443.
[14] Y. Wang, Q. Zhang, Y. Ohishi, T. Shishido, K. Takehira, Catal. Lett. 72 (2001) 215.
[15] Q. Zhang, Y. Wang, Y. Ohishi, T. Shishido, K. Takehira, J. Catal. 202 (2001) 308.
[16] W. Schuster, J.P.M. Niederer, W.F. Hoelderich, Appl. Catal. A 209 (2001) 131.
[17] S. Ge, C. Liu, S. Zhang, Z. Li, Chem. Eng. J. 94 (2003) 121.
[18] F. Dury, M.A. Centeno, E.M. Gaigneaux, P. Ruiz, Catal. Today 81 (2003) 95.
[19] P. Michorczyk, J. Ogonowski, Appl. Catal. A 251 (2003) 425.
[20] E.V. Kondratenko, M. Baerns, Appl. Catal. A 222 (2001) 133.
[21] G. Grubert, J. Rathousky, G. Schulz-Ekloff, M. Wark, A. Zukal, Micropor. Mesopor. Mater. 22 (1998) 225.
[22] M. Baltes, K. Cassiers, P. Van Der Voort, B.M. Weckhuysen, R.A. Schoonheydt, E.F. Vansant, J. Catal. 197 (2001) 160.

[23] X. Gao, I.E. Wachs, J. Phys. Chem. B 104 (2000) 1261.

[24] I.E. Wachs, Catal. Today 27 (1996) 437.

[25] I.E. Wachs, J.-M. Jehng, G. Deo, B.M. Weckhuysen, V.V. Guliants, J.B. Benziger, S. Sundaresan, J. Catal. 170 (1997) 75.

[26] I.E. Wachs, in: J.J. Spivey (Ed.), Catalysis, The Royal Society of Chemistry, Cambridge, 1997, p. 37.

[27] N. Magg, B. Immaraporn, J.B. Giorgi, T. Schroeder, M. Bäumer, J. Döbler, Z. Wu, E. Kondratenko, M. Cherian, M. Baerns, P.C. Stair, J. Sauer, H.-J. Freund, J. Catal. 226 (2004) 88.

[28] C.-B. Wang, G. Deo, I.E. Wachs, J. Catal. 178 (1998) 640.

[29] X. Gao, S.R. Bare, B.M. Weckhuysen, I.E. Wachs, J. Phys. Chem. B 102 (1998) 10842.

[30] M.M. Koranne, J.G. Goodwin, G. Marcelin, J. Catal. 148 (1994) 369.

[31] F. Arena, N. Giordano, A. Parmaliana, J. Catal. 167 (1997) 66.

[32] H. Berndt, A. Martin, A. Brückner, E. Schreier, D. Müller, H. Kosslick, G.H. Wolf, B. Lücke, J. Catal. 191 (2002) 384.

[33] R. Zhou, Y. Cao, S. Yan, J. Deng, Y. Liao, B. Hong, Catal. Lett. 75 (2001) 107.

[34] J.L. Callaham, R.L. Grasselli, AIChE J. 9 (1963) 755.

[35] E.V. Kondratenko, M. Cherian, M. Baerns, Catal. Today 99 (2005) 59.